Experimental quantum non-Gaussian mechanical states of a trapped ion

a dissertation report

Lukáš Podhora

Palacký University Olomouc

2024

Title:	Experimental quantum non-Gaussian mechanical states of a trapped ion
Author:	Mgr. Lukáš Podhora
Supervisor	prof. Mgr. Radim Filip, Ph. D.
Advisor:	Mgr. Lukáš Slodička, Ph. D.
Study programme:	Optics and Optoelectronics
Institution:	Department of Optics, Faculty of Science, Palacký University
Year:	2024
External Examiners:	**Mgr. Juraj Fedor, Ph. D.** Department of Dynamics of Molecules and Clusters, J. Heyrovský Institute of Physical Chemistry **prof. RNDr. Pavel Zemánek, Ph. D.** Institute of Scientific Instruments, The Czech Academy of Sciences

The thesis is available at the study department of the Faculty of Science, Palacký University, 17. listopadu 12, 77146 Olomouc, Czech Republic. It is also available online at stag.upol.cz when searching the student's name. The defense will take place at the Department of Optics, Faculty of Science, Palacký University Olomouc, in spring or summer 2024.

I declare that I wrote this Thesis myself under the guidance of my supervisor prof. Radim Filip and my consultant dr. Lukáš Slodička. I declare that I personally performed all the presented experimental measurements at the trapped ion apparatus, which is located in the joined laboratory at Institute of Scientific Instruments, The Czech Academy of Sciences, Brno. Some text parts and figures for this Thesis were directly taken from our original published articles, where I contributed as a main author.

Olomouc
March 2024
Lukáš Podhora

Abstract

A single trapped ion has proved to be one of the most convenient physical systems to realize and experimentally control the quantum bit, which is implemented as a superposition of a two-level system between two distinct energy levels. Additionally, the perfect isolation from surrounding environment of a single ion in a Paul trap placed in vacuum chamber provides a way to experimentally realize the harmonic oscillator level scheme. Together, these two physical systems allow for experimental realization of Jaynes-Cummings and anti-Jaynes-Cummings interactions, which provide a deterministic control over the motional degree of freedom in means of atom-light interaction. Such experimental systems have already been proven useful for enhanced quantum sensing, quantum computation, quantum communication and other areas of recent scientific interest.

This thesis summarizes our experimental work devoted to generation and control over the non-classical quantum states of motion. The discrete building blocks of such states are the number states with exactly defined amount of energy. In the first presented experiment, we realize a generation of number states, with a main focus on characterization of their non-classical properties with respect to the controllable amount of added thermal energy. The crucial concept implemented to states' characterization is a 'quantum non-Gaussianity', which sets the limit on states achievable by application of any combination of coherent displacement or squeezing on a ground state. The results uncover that even for the sufficiently high amount of added thermal noise the crucial quantum non-Gaussian features are preserved, and such states can provide a significant enhancement of metrological sensitivity.

Additional two experiments present a novel method of non-classical states generation which takes advantage of the increasing initial thermal energy. The heart of the generation process lies in the repetitive application of Jaynes, or anti-Jaynes-Cummings interactions to the initial thermal state. The motional population eventually converges towards the determined mixture of discrete energy levels, a process which we denote as an 'accumulation'. By evaluation of criteria of non-classicality and quantum non-Gaussianity, we prove that the overall amount of the non-classical aspects in resulting states is clearly enhanced by the repetition of the deterministic interaction process and also by increasing energy of the initial thermal distribution.

Keywords: quantum state, quantum non-classicality and non-Gaussianity, Jaynes-Cummings and anti-Jaynes-Cummings interaction, trapped ion, mechanical oscillator

Anotace

Jednotlivé atomy držené v Paulově pasti patří k nejvhodnějších fyzikálních systémům pro experimentální kontrolu kvantového bitu, který je realizován jako superpozice dvouhladinového systému mezi dvěma rozdílnými energetickými hladinami. Dokonalá izolace atomu od okolního prostředí v Paulově pasti umístěné ve vakuové komoře umožňuje také realizovat hladinové schéma harmonického oscilátoru. Vzájemným provázáním pohybového stuplně volnosti a dvouhladinového systému vzniká možnost realizace Jaynes-Cummings a anti-Jaynes-Cummings interakcí, které poskytují deterministickou kontrolu pohybového stupně volnosti s využitím principů interakce záření a látky. Tyto experimentální interakce se ukazují jako užitečné pro vývoj kvantových sensorů, kvantovém počítání, komunikaci a v dalších oblastech souvisejícího výzkumu.

Tato disertace shrnuje naši experimentální práci věnovanou tvorbě a kontrole neklasických kvantových stavů pohybu. Základem těchto stavů jsou číselné stavy pohybu s přesně definovanou energií. V prvním z prezentovaných experimentů realizujeme generaci těchto číselných stavů a zaměřujeme se především na charakterizaci jejich neklasických vlastností v souvislosti s množstvím přidané tepelné energie. Klíčovým konceptem použitým k charakterizaci vytvořených stavů je ”kvantová ne-Gaussovost”, která určuje, jestli je možné dané pohybové stavy vytvořit pomocí kombinace koherentních operací nebo stlačení aplikovaných na základní stav. Výsledky experimentu ukazují, že i při výrazném množství přidaného tepelného šumu jsou klíčové ne-Gaussovské vlastnosti zachovány, a vytvořené stavy mohou poskytovat významné zvýšení metrologické citlivosti.

Další dva experimenty představují novou metodu generace neklasických stavů pohybu, která využívá počáteční termální energii vstupního stavu oscilátoru. Základním principem generace je opakovaná aplikace Jaynes nebo anti-Jaynes Cummings interakce na počáteční termální pohybový stav. Populace pohybových stavů směřuje k přesně dané směsi diskrétních energetických hladin, což je proces, který definujeme jako ”akumulace”. Výpočtem kritérií neklasičnosti a kvantové ne-Gaussovosti se podařilo dokázat, že celkové množství neklasických vlastností ve vytvořených stavech se zvyšuje s množstvím opakování interakce a také s rostoucí energií počátečního termálního stavu.

Klíčová slova: kvantový stav, kvantová neklasičnost a ne-Gaussovost, Jaynes-Cummings a anti-Jaynes-Cummings interakce, chycený ion, mechanický oscilátor

Acknowledgements

First and most of all, I want to thank Lukáš Slodička for almost ten years of our mutual collaboration during my Master's and Ph. D. studies. I am grateful for his guidance, patient mentorship, and for that he taught me all the experimental and theoretical methods to work in field of trapped ion quantum optics. I also appreciated our bike trips together, and our philosophical discussions during the laboratory work as well. Second, I thank Radim Filip for overseeing my Ph. D. studies, providing motivation and course to our published articles and teaching me lots about theoretical quantum physics.

I thank all the friends from our laboratory group in Brno. I thank Minh Tuan Pham for teaching me how to handle lasers and electronics in the lab, Adam Lešundák for experiments that we worked on together, Martin Čížek for handling and fixing the electronics and Daniel Babjak for measurements on fluorescence from ions that we did together.

I am grateful to my colleagues in Olomouc as well. Particularly, I want to thank Jaromír Mika for his continuous support, Petr Obšil, Dung Tran, Tomáš Lamich and Antonín Bekárek for collaboration on new trapped ion experiments in newly built laboratory in Olomouc. But most of all, I am grateful to Artem Kovalenko, who regularly traveled with me from Olomouc to Brno during the last year of my work, and helped me significantly to implement some of the presented experiments.

My thanks also belong to Barium team at university of Innsbruck, where I was privileged to spend a half year of my studies. Namely, I want to thank Gabriel Araneda and Giovanni Cerchiari for our cooperation in lab, Yves Colombe for theoretical discussions, prof. Rainer Blatt for giving me the opportunity to stay in his group, Vojtěch Krčmarský and Pavel Hrmo for friendly discussions and fun.

The greatest thanks belong to my wife Veronika, for her never ending support in all the difficulties, for her patience and for all the happy moments that we have lived together during the time of my studies. Thank You a lot!

List of publications

Publications covering results in this Thesis:

L. PODHORA, L. LACHMAN, T. PHAM, A. LEŠUNDÁK, O. ČÍP, L. SLODIČKA, AND R. FILIP, *Quantum Non-Gaussianity of Multiphonon States of a Single Atom*, Phys. Rev. Lett. **129**, 013602 (2022).

L. PODHORA, T. PHAM, A. LEŠUNDÁK, P. OBŠIL, M. ČÍŽEK, O. ČÍP, P. MAREK, L. SLODIČKA, R. FILIP, *Unconditional Accumulation of Nonclassicality in a Single-Atom Mechanical Oscillator*, Advanced Quantum Technologies **3**, 2000012 (2020).

A. KOVALENKO, D. BABJAK, A. LEŠUNDÁK, L. PODHORA, P. LACHMAN, P. OBŠIL, T. PHAM, O. ČÍP, R. FILIP, AND L. SLODIČKA, *Emergence of super-Poissonian light from indistinguishable single-photon emitters*, Optica **10**, 456-463 (2023).

P. OBŠIL, A. LEŠUNDÁK, T. PHAM, K. LAKHMANSKIY, L. PODHORA, M. ORAL, O. ČÍP, AND L. SLODIČKA, *A room-temperature ion trapping apparatus with hydrogen partial pressure below* 10^{-11} *mbar*, Review of Scientific Instruments **90**, 083201 (2019).

Publications based on results of internship in Innsbruck:

G. CERCHIARI, G. ARANEDA, L. PODHORA, L. SLODIČKA, Y. COLOMBE, AND R. BLATT, *Measuring Ion Oscillations at the Quantum Level with Fluorescence Light*, Phys. Rev. Lett. **127**, 063603 (2021).

G. CERCHIARI, G. ARANEDA, L. PODHORA, L. SLODIČKA, Y. COLOMBE, AND R. BLATT, *Motion analysis of a trapped ion chain by single photon self-interference*, Appl. Phys. Lett. **119**, 024003 (2021).

Articles based on Diploma Thesis research, published during my Ph.D. studies:

J. MIKA, L. PODHORA, L. LACHMAN, P. OBŠIL, J. HLOUŠEK, M. JEŽEK, R. FILIP AND L. SLODIČKA, *Generation of ideal thermal light in warm atomic vapor*, New J. Phys. **20**, 093002 (2018).

L. PODHORA, P. OBŠIL, I. STRAKA, M. JEŽEK, AND L. SLODIČKA, *Nonclassical photon pairs from warm atomic vapor using a single driving laser*, Optics Express **25**, 31230-31238 (2017).

Contents

1. Introduction

The term 'non-classical' state of motion in this work refers to the discrete energy distribution of motion incompatible with any mixture of displaced ground states of the oscillator [1]. We present several approaches where such nonclassicality can be controllably engineered with non-linear interactions. The 'quantum non-Gaussian' states represent the subclass of non-classical states that is beyond all mixtures of squeezed displaced oscillator ground states [2]. High quality quantum non-Gaussian states are in most experimental scenarios hard to prepare and observe. A well known property of a subclass of quantum non-Gaussian states is the negativity of the Wigner quasi-probability distribution function, however, it is not the necessary condition for the state to be non-Gaussian. In experiments considering single photons or the quantized motion in trapped atom, a specifically derived criteria can be conveniently used to characterize non-classical and non-Gaussian properties from the reconstructed population and detect them even in the presence of processes which destroy the negativity of Wigner function, such as losses or addition of thermal noise [3, 4].

Physically, the non-classical states of atomic motion can be employed in applications focused on experiments involving quantum metrology and quantum enhanced sensing [5–7], and quantum error correction [8–11]. It also finds it's applications in treating quantum engines [12, 13], or in simulation of many body interaction models and corresponding phase transitions [14].

The presented work focuses on engineering, measurement, and characterization of non-classical and quantum non-Gaussian states of motion, implemented on the mode of motion of single $^{40}\mathrm{Ca}^{+}$ ion held in a Paul trap. The non-classical properties of generated quantum states are evaluated from the measured distributions of motional populations. The presented results originate from three experiments, where two of them are already published in [15, 16], and the last measurement is currently being prepared for publication.

2. Mechanics with a trapped ion oscillator

2.1 Interaction of light with two-level atom in a harmonic potential

The fundamental principle of the motional state engineering lies in the interaction of the valence electron of an ion with light, which s sensitive to a motional state of an atom. In the Paul trap, the transition frequency of the two-level system is modulated by the frequency of the secular motion forming the modulation sidebands. These sidebands can be conveniently addressed with laser light while stabilizing, narrowing and fine-tuning the laser frequency, and in this way the motional energy can be added or subtracted. The complete Hamiltonian of such an interaction has a form

$$H = H_m + H_e + H_i, \tag{2.1}$$

where H_m describes the motional degree of freedom, H_e is the Hamiltonian of the two-level system, and the last part H_i describes the mutual interaction with light.

The light field providing the interactions between two-level and harmonic oscillator system can be treated as traveling electromagnetic wave, with the wavevector k, angular frequency ω and initial phase ϕ. Each interaction can be assigned with the physical quantity describing it's strength denoted as a Rabi frequency Ω [17, 18]. For the traveling light field and considering the electric dipole or quadrupole interaction, the interaction Hamiltonian can be found to be described by unified form, where we consider interaction with a single motional mode along x [17]

$$H^{(i)} = \frac{\hbar}{2}\Omega(|\mathrm{g}\rangle\langle e| + |e\rangle\langle \mathrm{g}|) \times [e^{i(kx-\omega t+\phi)} + e^{-i(kx-\omega t+\phi)}], \tag{2.2}$$

where the second bracket includes the electric field component of the laser propagating along the direction of the motional mode x. Here, the ω and ϕ are the frequency and phase of the excitation laser beam at the position of atom.

The transformation into the interaction picture is then expressed as

$$H_{\mathrm{int}} = U_0^{\dagger} H^{(i)} U_0, \tag{2.3}$$

where $U_0 = \exp[-(i/\hbar)H_0 t]$ is the unitary transformation and H_0 denotes free Hamiltonian $H_0 = H_m + H_e$. In the rotating wave approximation where the rapidly oscillating frequency components are dropped [17], the H_{int} becomes

$$H_{\text{int}}(t) = \frac{\hbar}{2}\Omega_0\sigma_+ \exp[i\eta(ae^{-i\nu t} + a^\dagger e^{i\nu t})]e^{i(\phi-\delta t)} + H.c., \tag{2.4}$$

with δ being the detuning from the transition frequency, H.c. is the Hermitian conjugate and Rabi frequency Ω_0 [17]

$$\Omega_0 = \frac{\Omega}{1 + q_i/2}, \tag{2.5}$$

where q_i is the stability parameter of the trap.

Here, we have used the raising and lowering operators $\sigma_+ = |g\rangle\langle e|, \sigma_- = |e\rangle\langle g|$, having the physical meaning of adding and subtracting energy in the two-level system. Additionally, we have defined the Lamb-Dicke parameter η as

$$\eta = \frac{2\pi}{\lambda}\sqrt{\frac{\hbar}{2m\omega}}, \tag{2.6}$$

which defines the ratio of the size of mechanical oscillation wavepacket with frequency ω with respect to the wavelength of the involved two-level system transition. Physically, the Lamb-Dicke parameter describes the relative interaction strength of coupling of the light to motional modes compared with its coupling to the carrier two-level transition where the motional change is not involved. Additional step towards simplification of the Hamiltonian 2.4 takes advantage of the Lamb-Dicke regime, where

$$\eta^2(2\overline{n} + 1) \ll 1. \tag{2.7}$$

Here, $\overline{n}$ stands for the mean value of the energy distribution of involved motional mode. Physically, in the Lamb-Dicke regime, all the transition involving transfer of more than single quantum in the motional mode are strongly suppressed. The interaction Hamiltonian can be expanded into the first order of η as

$$H_{\text{LD}}(t) = \frac{\hbar}{2}\Omega_0\sigma_+[1 + i\eta(ae^{-i\nu t} + a^\dagger e^{i\nu t})e^{i(\phi-\delta t)}] + H.c., \tag{2.8}$$

containing only three resonances for the values of $\delta = -\nu, 0, \nu$. For the case of $\delta = 0$ after the rotating wave approximation [17] the Eq. 2.8 results into 'carrier' transition, with the Hamiltonian

$$H_{\text{car}} = \frac{\hbar}{2}\Omega_0(\sigma_+ e^{i\phi} + \sigma_- e^{-i\phi}), \tag{2.9}$$

describing coupling to two-level system without affecting the motional degree of freedom, with ϕ denoting the phase factor corresponding to the laser phase. The detuning of laser from the carrier transition gives the second case, with $\delta = -\nu$, as

$$H_{\mathrm{rsb}} = \frac{\hbar}{2}\Omega_0\eta(a\sigma_+e^{i\phi} + a^\dagger\sigma_-e^{-i\phi}). \tag{2.10}$$

This interaction at the lower frequency is conventionally denoted with the term 'red sideband'. From the Eq. 2.10, it is apparent that the motional state is addressed simultaneously with the two-level system, where Lamb-Dicke parameter η plays the role of the 'coupling efficiency', defining the fraction of the original Rabi frequency Ω_0. Based on the initial state of the two-level system, the finite application of the interaction corresponding to H_{rsb} results in either subtraction of the single motional quantum while the two-level system being in state $|g\rangle$, or oppositely addition of quantum when the system is in $|e\rangle$.

The complementary regime, where $\delta = +\nu$ in Eq. 2.4, is described as

$$H_{\mathrm{bsb}} = \frac{\hbar}{2}\Omega_0\eta(a^\dagger\sigma_+e^{i\phi} + a\sigma_-e^{-i\phi}). \tag{2.11}$$

The H_{bsb} is denoted as anti-Jaynes-Cummings Hamiltonian, and the corresponding transition as a 'blue sideband'. We can denote the Rabi frequencies for couplings to higher and lower motional modes as $\Omega_{n,n+1}$ and $\Omega_{n,n-1}$, where the scaling is quantized with carrier Rabi frequency and the Lamb-Dicke parameter as

$$\begin{aligned} \Omega_{n,n+1} &= \Omega_0\eta\sqrt{n+1}, \\ \Omega_{n,n-1} &= \Omega_0\eta\sqrt{n}, \end{aligned} \tag{2.12}$$

which results from the properties of the annihilation and creation operators.

The dependence of the Rabi frequency on the motional distribution provides a key feature for engineering of the motional states and consequently for their readout. The Fig. 2.1 shows the visualizations of carrier, blue and red sideband interactions, as they result from the Eq. 2.8. The engineered interaction at blue sideband can be naturally employed to append the motional quanta into the oscillator, for the case that two-level system is in the ground state. On the contrary, the red sideband coupling provides a way for energy subtraction.

2.2 Coherent interaction on motional sidebands

The coherent Rabi oscillations denote the cyclic behavior of the population probability of the two-level system, undergoing the coherent drive. In implementations presented in this Thesis, they are observed either on carrier transition, which does not involve the interaction with motional mode of freedom, or at motional sidebands, which is

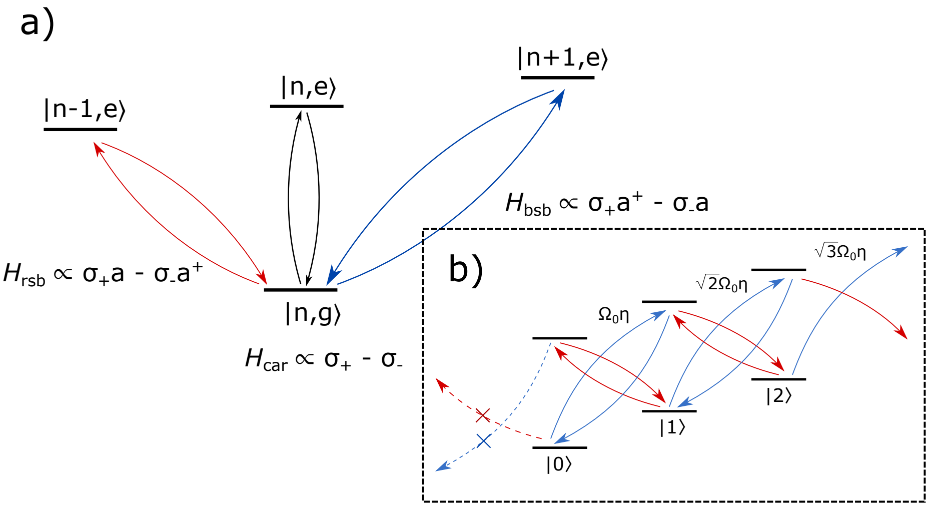

Figure 2.1: a) Visualization of the interactions for carrier (black), red sideband (red) and blue sideband (blue) for two-level system being initially in the $|g\rangle$ state. Hamiltonian H_{rsb} realizes the quantum subtraction between states $|n\rangle|g\rangle \leftrightarrow |n-1\rangle|e\rangle$, H_{car} does not affect the motional number, so that $|n\rangle|g\rangle \leftrightarrow |n\rangle|e\rangle$, and finally the blue sideband realizes transitions at $|n\rangle|g\rangle \leftrightarrow |n+1\rangle|e\rangle$. b) shows same two spin-motional coupling interactions, also pictured for additional higher energy levels. With the increasing energy, the initial Rabi frequency scales with the factor $\sqrt{n+1}$ for blue sideband and $\sqrt{n}$ for the red.

accompanied with an addition or subtraction of the single quantum. In such a case, the condition on sideband-resolved regime has to be fulfilled, meaning that the frequency of the motional mode is much larger than the natural linewidth originating from the spontaneous decay rate (so that $\omega \gg \Gamma$, where we consider ω on the scale of 10^6 Hz and $\Gamma \approx 1$ Hz for quadrupole transitions) [19]. Consequently, the Rabi oscillations are more conveniently observable at quadrupole 729 transition, due to the long lifetime of the excited state.

Additionally, we consider coupling in the Lamb-Dicke regime, which restricts the possible interactions to 1st motional sideband only, neglecting the higher order motional modes. With an ion prepared close to the motional ground state, there are only three achievable interactions, that being carrier, 1st red and 1st blue sideband, as described in Sec. 2.1. Following this treatment we describe the dynamics of the two-level system at carrier transition as an evolution of population probability of the excited state [19]

$$P_e(\tau) = \frac{1}{2}[1 - \sum_{n=0}^{n_{\max}\to\infty} P_n \cos(\Omega_0(1-\eta^2 n)\tau)], \tag{2.13}$$

where the sum is evaluated over the distribution of the motional modes P_n with $n_{\max} \to \infty$ being the maximal considered motional energy level, theoretically approaching infinity. For evaluations on measured data, the value of $n_{\max}$ is set sufficiently high, so it does not significantly affect the resulting population distribution.

The multiplication of the Rabi frequency Ω_0 with the square of Lamb-Dicke parameter η^2 points to the weak dependence of carrier coupling on the populations. The increasing thermal population in higher phonon states described with the element P_n is then responsible for the gradual damping of the Rabi oscillation, which can originate from contribution of axial and both radial motional modes. For thermal state, where P_n is described with Bose-Einstein distribution, the damped carrier Rabi oscillation pattern can be also expressed as following [19]

$$P_e(\tau) = \frac{1}{2}(1 - \frac{\cos(\Omega_0\tau) + \Omega_0\tau\eta^2(\overline{n}+1)\sin(\Omega_0\tau)}{1+(\Omega_0\tau\eta^2(\overline{n}+1))^2}), \tag{2.14}$$

where $\overline{n}$ determines the mean energy of the single motional mode. The Eq. 2.14 can be also extended to describe the damping originating from other motional modes, by replacing $\overline{n}$ and η with the summation over all motional modes and their corresponding Lamb-Dicke parameters [19].

The coupling to 1^{st} order motional modes at red or blue sideband contains both the frequency dependence on the Lamb-Dicke parameter η and the Rabi frequency Ω_0. The excited state probabilities $P_e^{\mathrm{bsb}}(\tau), P_e^{\mathrm{rsb}}(\tau)$ for 1^{st} blue and red sidebands are directly dependent on phonon probability distribution P_n as following

$$P_e^{\mathrm{bsb}}(\tau) = \frac{1}{2}[1 - \sum_n P_n \cos(\Omega_{n,n+1}\tau)\exp(-\gamma_n\tau)], \tag{2.15}$$

$$P_e^{\mathrm{rsb}}(\tau) = \frac{1}{2}[1 - \sum_n P_n \cos(\Omega_{n,n-1}\tau)\exp(-\gamma_n\tau)], \tag{2.16}$$

with

$$\Omega_{n,n+1} = \Omega_0\eta\sqrt{n+1}, \Omega_{n,n-1} = \Omega_0\eta\sqrt{n}, \tag{2.17}$$

where the coefficient γ_n describes the Rabi oscillation damping which is dependent on the energy of the motional mode denoted with n. In our experimental observations and also in references [17, 20] it has been found that the damping coefficient scales up with the motional energy and can be described as

$$\gamma_n = \gamma_0(n+1)^x, \tag{2.18}$$

with γ_0 is the damping of the motional ground state, and x is the scaling factor which is related with the noise properties, typically estimated as $x = 0.7$, see reference [20].

2.3 Basic definitions of non-classicality in ion's motion

There are two basic ways to treat the quantum mechanical motional states. The first treatment employs the decomposition of arbitrary state in the number state basis. Alternatively, the motion can be treated similarly as in quantum optics, using the theory of coherent states, firstly introduced by Glauber in 1963 [1]. In this way, the density matrix of the state can be described as [21]

$$\rho = \int P(\alpha) |\alpha\rangle \langle\alpha| \, d^2\alpha, \tag{2.19}$$

where the outer product $|\alpha\rangle\langle\alpha|$ denotes the over-complete non-orthogonal basis of coherent states. By definition in [21], if $P(\alpha)$ has meaning of classical probability density function, then state is classical from the perspective of classical coherence theory of linear oscillators. Such states can be obtained by classical external linear drive of such oscillators with a fixed frequency. If this is not the case, the state is called 'non-classical'. The special subclass of non-classical states presents sub-Poissonian statistical properties where the variance in phonon number is smaller than the mean phonon number [22]. This is also the case of Fock mechanical states, where the phonon number noise is principally zero, while the phase is infinitely uncertain. However, such noise reduction can be also approached by a displaced squeezed ground states of oscillators. They can be obtained using diverse linearized nonlinear dynamics described approximately by the interaction Hamiltonians maximally quadratic in the annihilation and creation operators. Such dynamics ideally keeps Gaussian ground-state distributions of position and momentum still Gaussian. To basically distinguish such trivial cases on sub-Poissonian statistics from more relevant and applied still imperfect Fock states, quantum non-Gaussian sub-set of non-classical states must be introduced.

Similarly with the definition in Eq. 2.19, we define the 'quantum non-Gaussianity' with use of the following equation [2]

$$\rho = \int P(\lambda) |\lambda\rangle \langle\lambda| \, d^2\lambda, \tag{2.20}$$

where $|\lambda\rangle = S(r)D(\alpha)|0\rangle$ is a pure Gaussian state, with displacement operator $D(\alpha)$, squeezing $S(r)$ and $|0\rangle$ denoting the vacuum state. In Eq. 2.20, the $P(\alpha)$ denotes the probability density distribution of Gaussian states $|\lambda\rangle$. In case that the quantum state cannot be described in a way of Eq. 2.20, it is denoted as 'quantum non-Gaussian'.

A convenient way to characterize the quantum states is the direct reconstruction of number states population, where for example the Fock state probabilities may be directly obtained from the fit of the coherent interaction (see Eq. 2.15). A specific criteria has been derived [2], which distinguishes Gaussian and quantum non-Gaussian states based solely on the measured populations, and can be applied even in the presence of high losses or for states with positive Wigner functions in whole phase space.

The stricter form of quantum non-Gaussianity criteria can be formulated using the hierarchical properties of the Fock states, which directly relate to some of the sensing applications. The hierarchical nature of the criteria also provides a way to gradually describe the 'quality' of generated imperfect Fock states, by evaluating their robustness with respect to thermal losses, which is specific for each Fock state. The genuine quantum non-Gaussianity (GQNG) is defined similarly to quantum non-Gaussianity (QNG), with the Eq. 2.20, where $|\lambda\rangle = S(r)D(\alpha)\sum_{m=0}^{n-1} c_m |m\rangle$ denotes the sum of coherent and squeezing operations applied on the mixture of number states with order $(n-1)$ smaller than the number state of interest. Therefore, the GQNG state is such state, which cannot be expressed with a mixture of displaced and squeezed number states of a lower rank. A specific $P_n^{\max}$ can be derived for each number state, for witnessing the GQNG threshold. In a single term, the genuine quantum non-Gaussian state of rank n can be defined as a state, which cannot be achieved by

$$|\psi\rangle = D(\alpha)S(r)\sum_{m=0}^{n-1} c_m |m\rangle . \tag{2.21}$$

Alternatively, it is possible to derive the condition for genuine quantum non-Gaussianity for Fock states with use of stellar hierarchy formalism, as described in the reference [23].

3. Experimental methods to control ion's motion

3.1 Laser manipulation of internal energy level populations

The crucial point of the experimental control lies in addressing of the transitions between energy levels in the $^{40}Ca^{+}$ ion (Fig. 3.1). This is done by employment of in total four lasers. The description of the laser stabilization using frequency offset locks to the fiber frequency comb and including the particular set up for stabilization of the qubit 729 nm laser to the level of a few Hz can be found in [24, 25]. In addition, other two lasers at 422 nm and 377 nm are used to produce singly ionized $^{40}Ca^{+}$ion. At first, one of the two valence electrons is excited at transition $4s^2S_0 \rightarrow 4s4pP_1$ by 422 nm radiation, and in the second step, it is sent into continuum by laser at 377 nm.

The transition $4S_{1/2} \rightarrow 4P_{1/2}$ is used for Doppler cooling and also for fluorescence detection, due to the short excited state lifetime which is 6.9 ns. The light of the fluorescing atom is collected with a high numerical aperture lens[1], which is then further sent towards the EMCCD camera[2], or to the avalanche photo-detector[3]. In typical experimental setting, it is possible to detect up to 4×10^4 photons per second.

In the cooling and detection process at $4S_{1/2} \rightarrow 4P_{1/2}$ transition, the finite branching ratio of the excited state results into a probability of decay into the metastable $3D_{3/2}$ state. Therefore, the reshuffling laser at 866 nm is employed to re-excite the atom into the $4P_{1/2}$, from where the electron may decay back to the ground level $4S_{1/2}$. The two beams at 397 nm and 866 nm have to be implemented simultaneously, in order to detect the ion's fluorescence and reduce the motion in Doppler cooling step.

The quadrupole transition at $4S_{1/2} \rightarrow 3D_{5/2}$ is addressed with the 729 nm laser beam. The lifetime of the excited $3D_{5/2}$ state is very long (1.16 s), so the 729 nm beam frequency has to be narrowed and stabilized to the bandwidth scale of approximately tens of Hz. This is achieved by PDH locking to a high finesse reference cavity, which is in detail described in work [25]. The transition between the states $3D_{5/2} \rightarrow 4P_{3/2}$ serves for the reshuffling of the excited D-state to the ground state $S_{1/2}$.

[1]Sill Optics S6ASS2241, covering 2 % of full solid angle [24]
[2]ANDOR Luca, type S
[3]Laser Components COUNT Blue

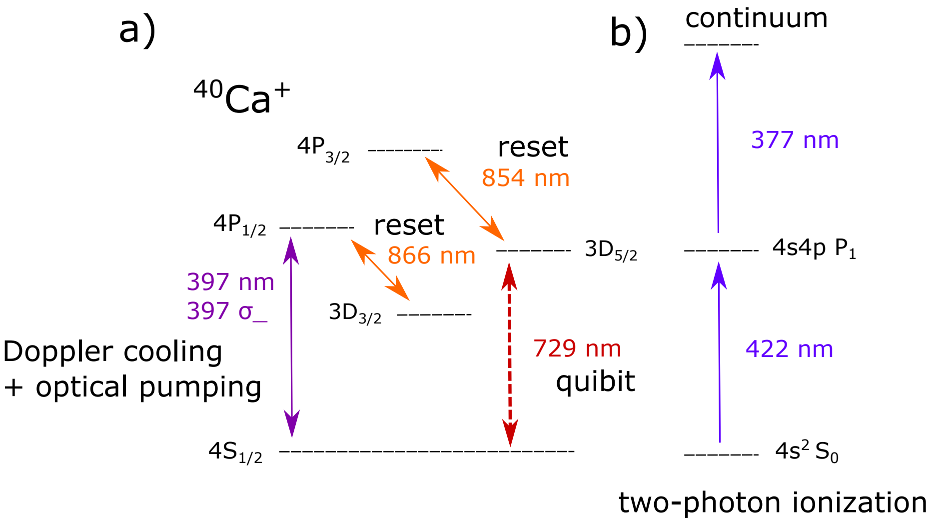

Figure 3.1: Processes of electronic state manipulation used in experiments. a) shows spectral lines for experimental control and motional manipulation. The fluorescent 397 nm transition serves for Doppler cooling and also for optical pumping with circularly polarized beam. 866 nm serves for the re-shuffling of the dark state $3D_{3/2}$ after Doppler cooling. The narrow quadrupole 729 nm transition defines the two-level system coupled with the harmonic oscillator. The beam at 854 nm serves for a reshuffling of the $3D_{5/2}$ state down to the ground state $4S_{1/2}$. In addition, the special circularly polarized beam at 397 nm denoted as σ^- is used to distinguish transitions corresponding to two Zeeman levels of $4S_{1/2}$ ground state. b) shows the two-photon ionization process used for ion trapping.

The geometric orientation of the laser beams with respect to the trap is depicted in Fig. 3.2. The orientation takes into account the geometry of direction of normal oscillation modes in the trap. The beams which are aligned under 45° angle have a significant overlap with all of the three motional modes of a single ion. This direction is used both for the Doppler cooling lasers and for the qubit laser. The 397 σ_- beam, denoted as 'optical pumping', propagates parallel to the trap axis. The beam is circularly polarized, and it's direction coincides with the local magnetic field vector. This ensures that only one of the two Zeeman levels of the ground state $S_{1/2}$ can be coupled [26, 27].

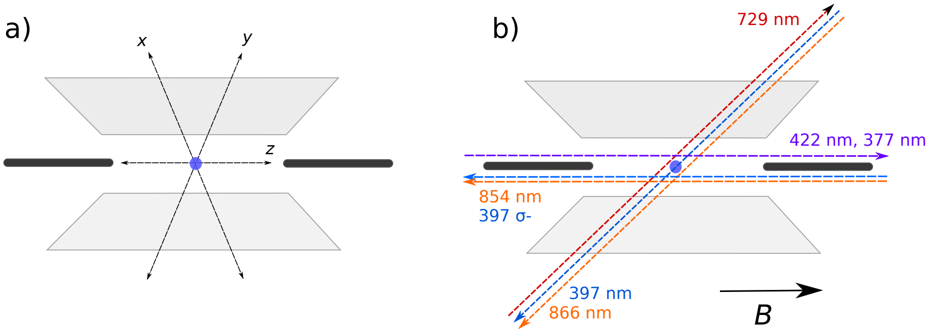

Figure 3.2: Geometry of normal motional modes in the trap and alignment of the laser beams. a) shows the three main directions of oscillations, where x, y represents two radial modes which are bound to two pairs of 'blade' electrodes (only one pair is shown here), z is the direction of the axial mode. b) depicts the alignment of lasers used for internal state control and two-photon ionization process, with respect to trap axes. A Doppler cooling is performed with 397 and 866 nm lasers, 729 nm provides tools for the motional state engineering, 377 and 422 nm lasers implement the ionization step, 397 σ^- does the optical pumping and 854 nm re-shuffles the excited state level. For the description of the typical pulse sequence, see Sec. 3.2. The direction of the magnetic field depicted with B is set as parallel to the axis of the trap in all experiments presented in this thesis, which allows for a convenient optical pumping scheme with the 397 circullary polarized beam along the trap axis.

3.2 Pulsed sequence control

The electron shelving method provides the projection to one of the eigenstates of the two-level system. Despite the actual superposition, the single shelving experiment always returns a yes/no answer, if the atom was in the 'dark' or 'bright' state. Therefore, any experimental sequence is implemented with a high number of repetitions, which allows to obtain the statistics of projections on the two-level system. The sequences of excitation laser pulses are directed with the programmable RF-generator[4] and from here, pulses are delivered to the set of acousto-optical modulators[5]. All the experiments consist of a hundred independent sequence repetitions, which suppress the projection noise and provide the probability amplitudes with the reasonable error estimate.

A general form of the sequence is depicted in Fig. 3.3. The sequence starts with the Doppler cooling, followed with optical pumping, possibly sideband cooling which further reduces the mechanical thermal energy, then with state manipulation and

[4] electronics based on FPGA logic, controlled in LabView software

[5] Brimrose, central frequency of modulation typically 250 MHz

finally the state analysis.

3.3 Engineering motional quantum states

The aim of the motional state engineering in this Thesis is to control the phonon number distribution P_n in such way, that we are able to construct a state with desired statistical distribution of interest. We will not consider coherent aspects of generated phonon superpositions and focus solely on the phonon number probabilities. The methods to achieve so lie either in setting of the length of Doppler and sideband cooling, leading to generation of classical states with thermal distributions, or by setting the arbitrary combination of carrier and first order motional sideband pulses. We will focus here on basic methods of generation and population reconstruction for thermal and Fock states of motion, and their statistical mixtures resulting from a mechanical thermalization or deterministic nonlinear manipulations of thermal states.

3.3.1 Thermal states

A thermal state of motion can be simply achieved by laser cooling. Statistics of phonon populations P_n after cooling typically obeys the Bose-Einstein thermal distribution [17, 28, 29] written as

$$P_n = \sum_n \frac{\overline{n}^n}{(\overline{n}+1)^{n+1}}. \tag{3.1}$$

which is characterized with a single variable $\overline{n}$ denoted as mean energy. The amount of mean thermal phonon population $\overline{n}$ can be tuned by length of the sideband-cooling sequence in the state preparation step. In this way, the energy may be tuned from a close-to ground state, up to the Doppler cooling limit. Particularly, for our experiment, the scope lies between $\overline{n} = 0.03$ up to $\overline{n} \approx 8$.

The characterization of the thermal motional distribution shrinks to the aim of finding the mean energy $\overline{n}$ and confirmation of the thermal character of the observed photon probability distribution. There are various methods to achieve so, including comparison of couplings to red and blue sidebands [17, 30], measuring of the strength of motional coupling with respect to the carrier transition [19], or measuring the spatial and coherence properties of emitted light. They include the implementation of thermometry based on the optical spatial resolution of ion wavepacket [31], or related optical interferometric schemes [32]. However, for thermal state energy which is close to the Doppler cooling limit and lower, and in tight trapping potentials corresponding to motional frequencies on the order of a few MHz, the most convenient way of characterization is a direct fit of Rabi oscillations with the Eq. 2.15.

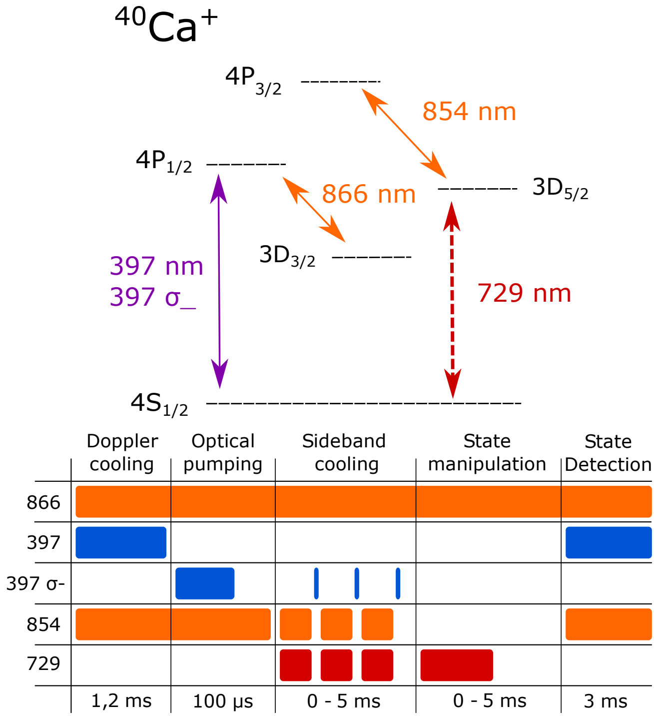

Figure 3.3: Example of the experimental sequence used for motional state preparation, manipulation and state detection. The Doppler cooling represents the continuous illumination with 397 nm and 866 nm lasers, typically with 1.2 ms duration. The optical pumping initializes the state of the electron to particular m_j state of the S state. The sideband cooling part consists of multiple pulses of simultaneous 729 nm and 854 nm beams, which are interrupted with short 397 σ_- optical pumping, preventing the population to accumulate in unwanted Zeeman component of the S state through rare decay of the excited $P_{3/2}$ state to $D_{3/2}$ followed by the optical reshuffling using 854 nm laser back to the S state manifold. The overall length of the sideband cooling sequence part depends on application. For ground state cooling with over 98 % of population in the state $|n\rangle = 0$, the required length exceeds 3 ms. State detection refers to the electron shelving, and also contains the gating of window for detection by the APD.

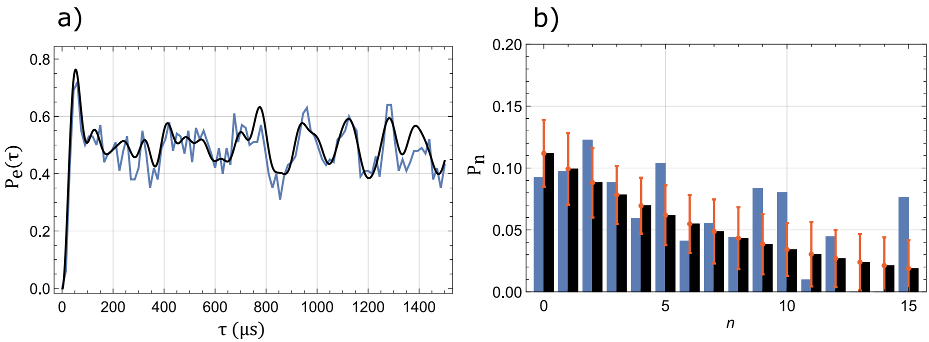

Figure 3.4: a) Blue sideband transition $4S_{1/2}(m = -1/2) \rightarrow 3D_{1/2}(m = -1/2)$ at axial motional mode measured at the limit of Doppler cooling, which is the initial state before application of the sideband cooling step. The state is prepared by application of 1 ms of Doppler cooling sequence step (see Fig. 3.3). The mean phonon number is estimated $\overline{n} = 8.0 \pm 1.0$. Blue trace presents the measured data, black is the fit from Eq. 2.15 with measured $\overline{n}$. b) shows the corresponding measured population (in blue), and theoretically estimated one (black), for the measured curves displayed in a). Fidelity of the populations from the full p_n fit with respect to theoretical was estimated as 78.5 %. The red error bars correspond to one standard deviation, which is evaluated for each population with use of the Monte-Carlo simulation method, assuming the projection noise from 100 population measurements on the two-level system. The resulting uncertainty of each population varies between ± 2.2 % to ± 2.9 %, with the average value ± 2.4 %. Comparison of measured data with these uncertainties shows that most of the values fall into to the interval defined by single standard deviation of the ideal value for corresponding thermal state, which implies that the Monte-Carlo estimation proves itself as a good method to estimate the uncertainty in case that it is not possible or convenient to perform repetitive measurements.

3.3.2 Number states

The experimental sequence for generation of the previously observed low number states $|g, 1\rangle$ and $|g, 2\rangle$ goes as following. We experimentally determine the exact length of the π-pulse by scanning the pulse duration in order to reach the most effective excitation to the $|e, 1\rangle$ level. Next, the π-pulse on carrier transition transfers the population back to the ground state of two level system, $|e, 1\rangle \rightarrow |g, 1\rangle$. In the last step, we apply a 854 nm quenching pulse, which serves to eliminate the residual population of the state $|e, 1\rangle$, which is typically much below 5 %. We also apply a short optical pumping pulse at σ_{-} at 397 nm to suppress the accumulation of the population in the $4S_{1/2}(m = +1/2)$ level, which can arise from the improbable $4P_{3/2}(m = +3/2) \rightarrow 3D_{3/2}(m = +3/2)$ decay.

In order to generate higher order Fock states, one may choose the method which extrapolates the sequence for the generation of $|2\rangle$, that is, iterative excitation of blue

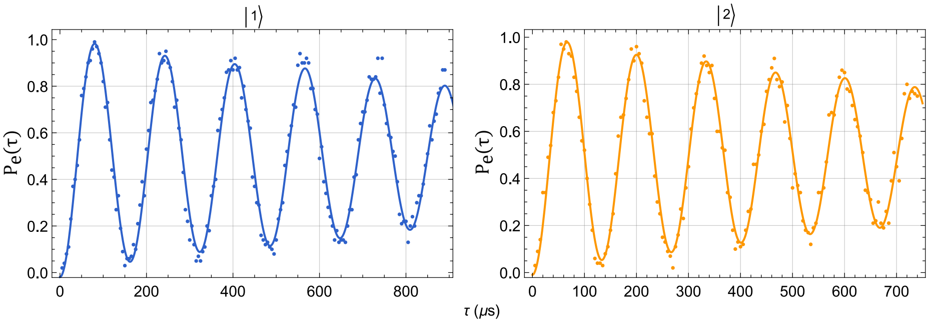

Figure 3.5: Fock states of motion at axial mode up to order $|2\rangle$, generated by the method of alternate application of blue and red sideband π pulses. The ground state Rabi frequency for this measurement was measured for ground state as $\Omega_0 = (2\pi \times 71)$kHz. For these values the populations of the measured number states was $P_1 = 0.96 \pm 0.02$ for state $|1\rangle$ and $P_2 = 0.98 \pm 0.02$ for state $|2\rangle$. The increase of motional number for the measured oscillations is manifested by the higher Rabi flopping frequency.

and red sidebands with pulse lengths corresponding to π pulses. In order to end up in the ground state of the electronic transition, the last pulse for the odd number state is the carrier π pulse, or a red sideband π pulse for even Fock states, respectively.

In Fig. 3.5, we plot the Rabi oscillations for generated Fock states $|1\rangle$ and $|2\rangle$. The frequency of the oscillation increases by the factor $\sqrt{n+1}$, which leads to shortening of the corresponding oscillation period. In order to maximize the amount of population transferred between the $|g, n\rangle \rightarrow |e, n+1\rangle$ states (or between $|e, n\rangle \rightarrow |g, n+1\rangle$ states), the duration of the π pulse is optimized experimentally by scanning the pulse duration. This is important due to the time offset of the RF pulse generated by the programmable pulse sequencer, which in our case slightly varies depending on the complexity of the pulse sequence. Also, the oscillation damping and loss of contrast slightly shift the position of the pulse maximum. he experimentally measured π pulses differ from theoretically estimated lengths by $\pm 5\ \mu s$.

4. Mechanical Fock states of single trapped ion

4.1 Heating dynamics for number states

For the short time scales of the experimental sequence, relevant for the generation of target Fock states, the heating results in the error given predominantly by values of (P_n, P_{n-1}, P_{n+1}). The QNG robustness may be thus conveniently characterized by a simple comparison of the amount of population P_n with respect to the populations contained in neighboring states P_{n-1}, P_{n+1}, with the QNG threshold probability defined as $(P_n, P_{n-1} + P_{n+1})$. In case that the population of state undergoing heating exceeds these values, it can be shown that the state may be described as Gaussian [4]. The depth of non-Gaussianity can be then understood as an amount of thermal noise, which can be added to the system and at the same time, the state population is higher threshold.

Figures 4.1 and 4.2 show the measured heating dynamics of the Fock states $|1\rangle$ and $|2\rangle$, respectively, illustrating the gradual thermal diffusion of the number state population towards the neighboring oscillator levels. For the measurement, we set the intensity of the Doppler heating pulse as in the calibration measurement, and we take the calculated heating into the simulation of the evolution probability. Both measured states show the slight asymmetry of diffusion favoring the higher motional states for short thermalization times. This is caused by the asymmetry in relative amplitudes for annihilation and creation operations. In Fig. 4.1, we observe the development of the Fock state $|1\rangle$ to nearly ideal thermal population distribution ($\overline{n} = 2.6$), however, it is still far from reaching the limiting Doppler temperature. For the limiting case of infinite heating time, we except the convergence to the ideal thermal state with a temperature corresponding to the Doppler cooling limit.

The same measurement results are also plotted in Fig. 4.3 in coordinates defined with $(P_n, P_{n-1} + P_{n+1})$. Here, the point located in the upper left corner denotes the initial state, and the heating proceeds towards the bottom right corner. The green ticks and red crosses denote the area, where the corresponding quantum states fulfill the GQNG condition, or reject it, respectively. While probing the state $|1\rangle$, the GQNG threshold is exceeded up to the thermalization pulse of the length $\tau = 2.1\ \mu$s, which adds the energy equal to $\overline{n} = 0.31$ phonons. For the state $|2\rangle$, the thermal depth of

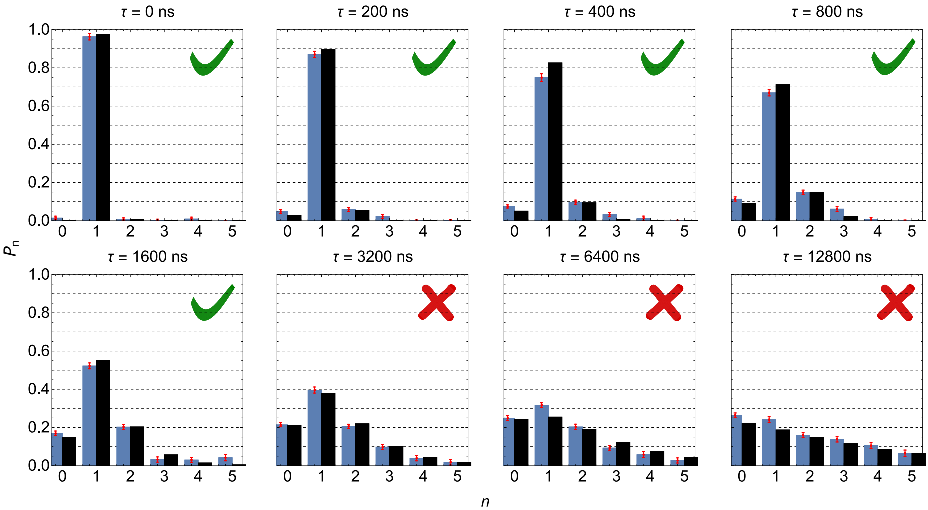

Figure 4.1: Heating dynamics and GQNG depth measured for Fock state $|1\rangle$. States which are marked with a green tick agree with the definition of the GQNG states (Eq. 2.20). States denoted with the red cross do not exceed the GQNG threshold. The limiting maximal amount of thermal energy which can be added to the system, and at the same time it preserves the QNG property, is estimated as $\Delta\overline{n} = 0.31$ phonons, corresponding to 2.1 μs heating pulse.

QNG is substantially lower, reaching $\overline{n} = 0.13$ phonons.

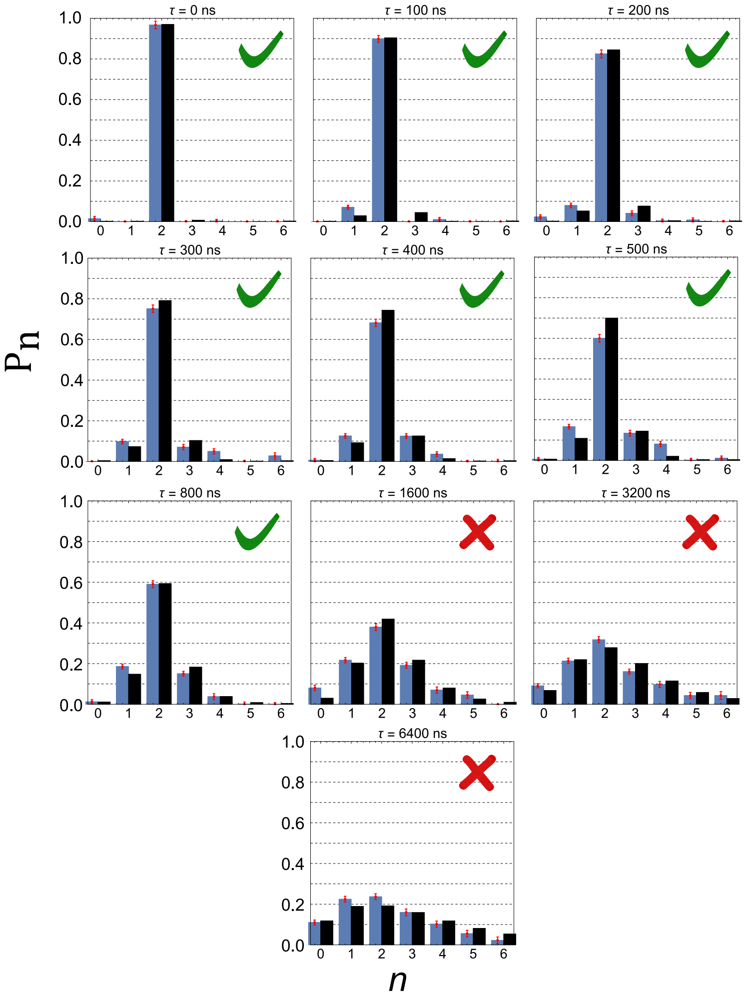

Figure 4.2: Measured thermalization dynamics and GQNG depth for Fock state $|2\rangle$. Similarly to the measurement in Fig. 4.1, the states marked with green tick are probably genuine QNG, while the states with red cross do not surpass the the GQNG threshold. The GQNG depth parametrized by the amount of added thermal energy is estimated as $\Delta\overline{n} = 0.13$, which is smaller when compared to $\Delta\overline{n} = 0.31$ for a number state $|1\rangle$.

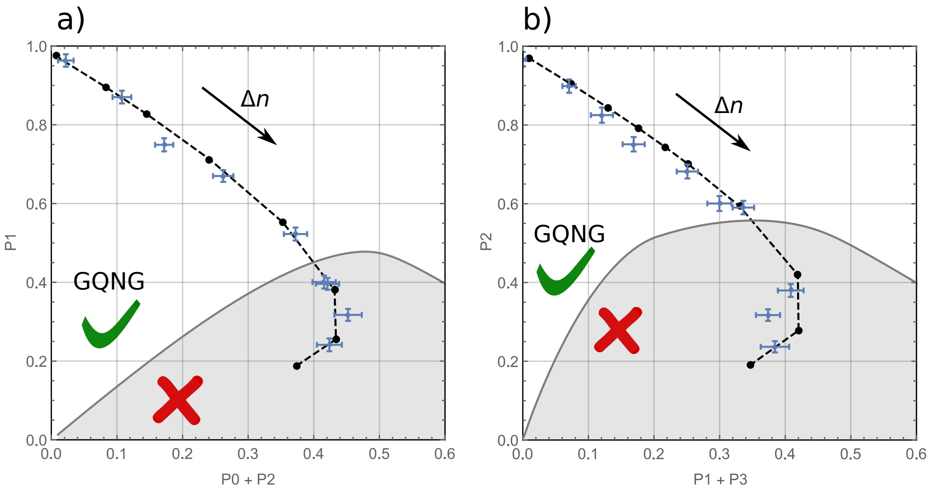

Figure 4.3: Thermalization dynamics for generated Fock states $|1\rangle$ in a), and $|2\rangle$ in b). Blue points correspond to measured states, and black line predicts a theoretical development, which corresponds to the state's distribution undergoing the addition of thermal energy according to the calibration measurement on the motional ground state. The dynamics progresses from the left upper corner, proceeding to the bottom right. The GQNG thermal depth for the number state $|1\rangle$ is evaluated as $\overline{n}_{\text{th}} = 0.31$ phonons, while for the state $|2\rangle$ this value is substantially lower, equal to $\overline{n}_{\text{th}} = 0.13$ phonons.

5. Deterministic accumulation of non-classicality

5.1 Phonon addition in anti-Jaynes-Cummings interaction

The experimental conditions are similar to those in the experiment described in Chapter 4. The axial motional mode frequency has been set to $\nu_{\mathrm{ax}} = 1.188$ MHz. The carrier Rabi frequency was measured as $\Omega_c = 2\pi \times (92 \pm 1)$ kHz and the Lamb - Dicke parameter $\eta_{729} = (61.1 \pm 0.2) \times 10^{-3}$. The optimized π pulse length was measured as $\tau = 91\ \mu s$.

The experimental sequence follows with sideband-cooling step, where a variable pulse duration is used to tune the initial thermal energy. In a motional manipulation step, we apply the single 729 nm pulse with length τ to the 1^{st} blue motional sideband, which adds the energy given by the pulse area gt. A short 854 nm reshuffling pulse is applied to transfer the residual D-state population back to the ground state of a two-level system. The state readout is performed with the electron shelving method, realizing hundred repetitions of the experimental sequence. The resulting population distribution is then obtained by a fit of the blue sideband Rabi oscillations using the Eq. 2.15.

In the first measurement we prove that, already for an initial state having a thermal Bose-Einstein population distribution, the incoherent modulation deterministically results into the non-classical states even for a broad range of initial thermal energies. The pulse area gt is in this case set as $gt = \Omega_0 \eta \tau = \pi/2$, which is experimentally calibrated at 1^{st} blue sideband excitation of $|g,0\rangle \rightarrow |e,1\rangle$. While varying the initial thermal energy $\overline{n}$, we add a phonon depending on the chosen gt and input state statistics which leads to a transfer of a whole population from P_0 to P_1 for an ion prepared initially in the motional ground state.

The resulting statistics of initial thermal states and resulting distribution after the phonon addition are depicted in Fig. 5.1. The data measured after the interaction indeed show the obvious emergence of non-classical statistics with the benefit of P_1. The state with the lowest thermal energy corresponding to the ground state of motion was prepared such that $\overline{n}_{th} = 0.005 \pm 0.005$, and the corresponding population $P_0 = (99.5 \pm 0.5)\%$. The single phonon addition was measured to have an efficiency close to $\kappa = 97$ %, which corresponds to the maximum of the 1^{st} blue sideband

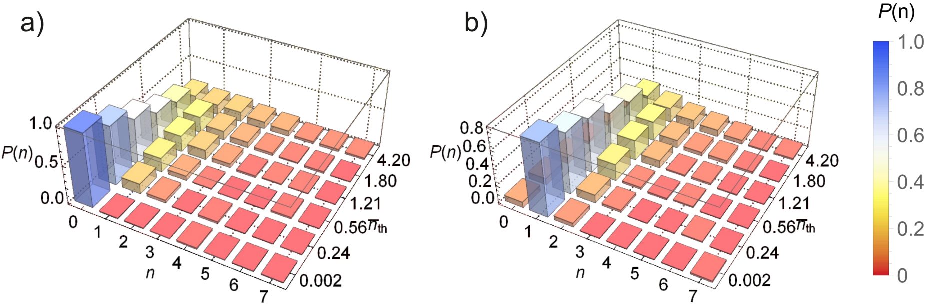

Figure 5.1: Measured distributions of initial thermal state, undergoing a an addition of a single quantum at AJC interaction with $gt = \pi/2$, which would ideally correspond to the transformation of the whole population from the state $|g,0\rangle \rightarrow |e,1\rangle$. a) shows the reconstructed initial thermal states, b) depicts distributions after the addition of a single motional quantum. The axis denoted with n_{th} defines the mean energy of initial thermal state, axis n points out the population of corresponding number state level.

Rabi flop between the states $|g,0\rangle \rightarrow |e,1\rangle$. Additional imperfection in efficiency of the full phonon addition step arises form the reshuffling and optical pumping steps performed with 854 nm and 397 nm σ_- beams. This leads to approximately $(2.9\pm0.2)\%$ loss of P_1 population which diffuses through photon recoils towards the neighboring number states. The uncertainties of resulting populations are estimated with use of the Monte-Carlo routine, where the input uncertainties for each data point in the Rabi oscillations were sampled according to expected minimal noise - projection noise.

Next, we evaluate the criteria of non-classicality for different input thermal states after the single quantum addition. Fig. 5.2 shows results of the evaluation of Fano factor $F = \langle(\Delta n)^2\rangle/\langle n\rangle$, Klyshko's criteria for nonclassicality [33], function at the center of the phase space $W(0,0)$, for initial thermal states undergoing an addition of a single quantum with a BSB pulse area of $gt = \pi/2$. The non-classicality is proved by the negativity of measured first order Klyshko criteria K_1. The measured negative value of Winger function $W(0,0) < 0$ additionally proves the quantum non-Gaussian features for all the resulting states. Finally, the negative values of Fano factor point out to the convergence of the resulting statistics towards the sub-Poissonian distributions. We additionally evaluated the witness of quantum non-Gaussian properties based on the estimation of only two neighboring phonon number probabilities, P_1 and P_2. It unambiguously witnesses the QNG aspects for all input thermal states up to mean $\bar{n}_{th} = 4.2$, where the multi-phonon contributions are already too high. The measured states which fulfill the quantum non-Gaussian property are marked with the red tick in Fig. 5.2.

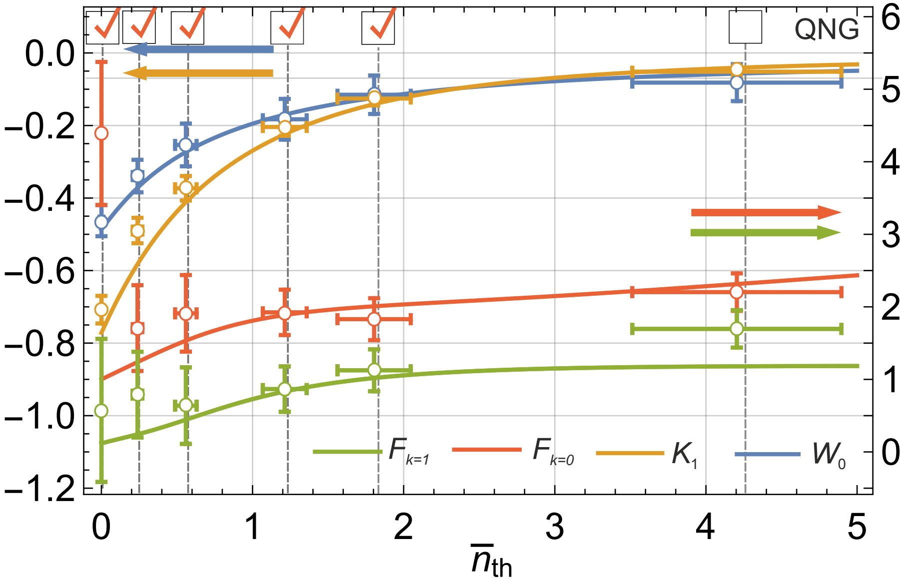

Figure 5.2: The results of evaluation of nonclassicality for the measured phonon number distributions after single nonlinear anti Jaynes-Cummings interaction of atomic mechanical oscillator prepared in thermal state. The Fano factors evaluated for initial and generated phonon populations demonstrate the conversion to sub-Poissonian statistics for states with low initial thermal energy $\bar{n}_{\text{th}}$. The evaluated negative Klyshko's criteria K_1 for each output distribution unambiguously confirm a strong nonclassicality of the generated states for a broad range of initial thermal energies $\bar{n}_{\text{th}}$. In addition, the observed negative values of the Wigner quasi-distribution $W(0,0)$ suggest that the generated state is always non-Gaussian. Moreover, quantum non-Gaussianity criteria (QNG) [3] show impact of multi-phonon contributions. The measures evaluated from the experimental data are displayed as full circles with error bars corresponding to three standard deviations.

6. Non-classical motional states from Jaynes-Cummings interaction

6.1 Experimental non-classical states in J-C interaction

The experimental sequence starts by preparation of the thermal motional state with energy $\overline{n} = 0.93 \pm 0.06$. The resulting populations are compared with ideal Bose-Einstein distribution reconstructed from the measured state's energy. The pulse area $gt = \pi$ is set by setting the pulse duration to $\tau = 272\ \mu$s. The pulse is applied on the 1^{st} red motional sideband. The phonon number statistics is reconstructed from the blue axial sideband with use of the Eq. 2.15. We repeat the phonon subtraction step up to $k = 5$ iterations, which is already sufficient for amplification of fundamental positive aspects of initial thermal energy.

For the experiment, ground state Rabi frequency was measured as $\Omega_0 = 2\pi \times (60.2 \pm 0.1)$ kHz, Lamb-Dicke parameter $\eta = (0.0611 \pm 0.0002)$ and ground state decay rate $\gamma_0 = 0.42 \pm 0.06$ kHz. A special attention is devoted for experimental estimation of pulse area gt, which has to be set to $gt = \pi$ with high accuracy. This value can be theoretically calculated from the measured Rabi frequency, however, due to the limiting offset in the response of employed electronic elements, the realistic length of the pulse is longer. Physically, the pulse area π corresponds to the whole period of the population transfer between the states $|g,1\rangle \rightarrow |e,0\rangle \rightarrow |g,1\rangle$ at red sideband, as depicted in Fig. 2.1. As the anti-Jaynes-Cummings interaction is described with the very same interaction strength $\eta\Omega_0$ when starting from the excited state, the similar process with exactly same interaction times is performed also on blue sideband as a cycle between the states $|g,0\rangle \rightarrow |e,1\rangle \rightarrow |g,0\rangle$. Therefore, the optimal interaction time $\tau = 272\ \mu$s corresponding to $gt = \pi$ pulse was estimated on the blue sideband and then applied to red sideband interaction from the state $|g,1\rangle$.

The probabilities are shown in Fig. 6.1 with blue columns. After the single interaction step, the process shows a significant enhancement of the population probability P_1. This effect is further amplified by repetitive interactions. The final measurement outcome after five iterations shows a clear convergence towards the states P_1 and P_4, which is in close agreement with a theoretical prediction. The most significantly populated states had probabilities $P_0 = 0.45 \pm 0.01, P_1 = 0.43 \pm 0.01$ and $P_4 = 0.08 \pm 0.02$. The third accumulation maximum, theoretically predicted at P_9, is not observable in this measurement due to the low initial energy. The error bars, corresponding to a single standard deviation, were statistically evaluated from five independent measurements of each state.

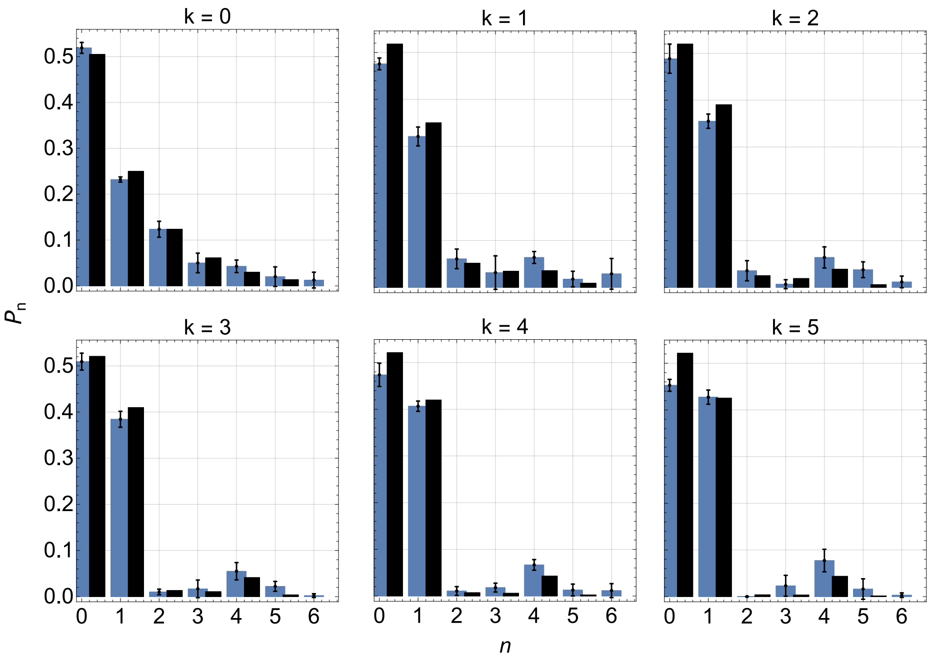

Figure 6.1: Reconstructed phonon distributions for initial thermal state with $\bar{n} = 0.93 \pm 0.06$ undergoing repetitive additions of energy $gt = \pi$ at red axial sideband. Here, n denotes the population level, P_n the occupation probability of the corresponding number state, and k describes the number of repetitive additions. Blue bars depict the measured data, black ones are values resulting from theoretical predictions.

The measured data in Fig. 6.2 clearly demonstrate the increase of the EP with number of phonon subtractions k applied to the initial thermal state. We measure the values of EP follow the predicted behavior within one standard deviation.

We probe the possible non-classicality by evaluation of Klyshko's criteria of non-classicality. Such a criteria can form a hierarchy dependent on n, where for each n exists a specific Klyshko criteria. For the current measurement, we evaluate the hierarchy up to the order 7, and depict the result in Fig. 6.2. The values of

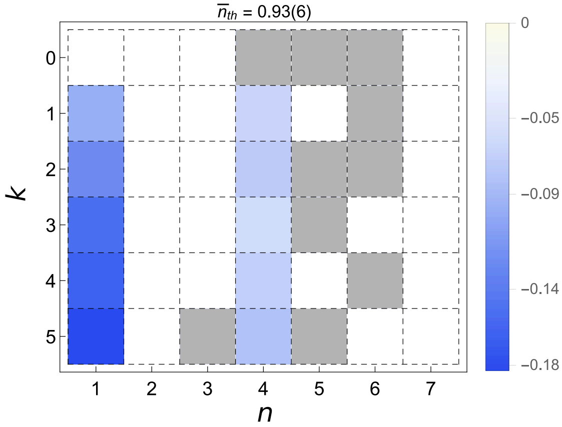

Figure 6.2: Evaluated hierarchy of Klyshko criteria K_n. The horizontal axis denotes the order of the Klyshko criteria n, the vertical line then number of accumulation pulses increasing from top to bottom. The columns related to P_1 and P_4 prove a clear non-classical nature of the generated states. The gray squares show the Klyshko parameter values, where we measured the negative values, but the negativity was smaller than single standard deviation. The white squares denote positions where the Klyshko parameter resulted positive.

K_1 and K_4 show a statistically significant amount of negativity. The negative value is apparent even after the single phonon subtraction, and gradually increases with the added accumulation steps. Physically, the negative value points to the fact that the occupation probabilities P_1 and P_4 are significantly larger than at least one of the neighboring oscillator states. The effect is much more pronounced for K_1, in agreement with the expectation of the dominant population of P_1 and suppressed population in P_2.

6.2 Thermally induced non-classical features

We explore the effect of phonon subtraction and accumulation for states with various initial thermal energies. We prepare five additional thermal states, which together with the already described measurement (Sec 6.1) form a set of total six measurements. For each initial thermal state, we perform the sequence of five repetitive subtractions, which became sufficient for enhancement of the observability of the target phenomena relevant for thermally stimulated nonclassicality.

The plot chart in Fig. 6.3 depicts the dynamics for three initial thermal energies. The rows represent low $\overline{n} = 0.14 \pm 0.03$, intermediate $\overline{n} = 2.0 \pm 0.1$ and high $\overline{n} = 2.9 \pm 0.3$ initial thermal energy. The first column shows the measured thermal distributions, the second one states after single interaction, and the third the distribution after $k = 5$ repetitive interactions. The data processing and simulations were performed following the recipe described Sec. 6.1.

In order to systematically evaluate the corresponding enhancement of nonclassical features of generated states, we evaluate the Klyshko hierarchy and entanglement potential measures. The hierarchy is depicted in the plot matrix in Fig. 6.4. The horizontal axis defines the order of the Klyshko criteria n which is under the probe. Vertical axis label refers to the initial thermal state $\overline{n}_{\mathrm{th}}$. The $k = 0$ refers to initial thermal states, $k = 1$ corresponds to a single absorption, and $k = 5$ to five cycles in total. The results show that for the increasing number of iterations, the negativity in Klyshko parameters K_1 and K_4 increases, pointing to the increasing non-classicality which is being accumulated in the system.

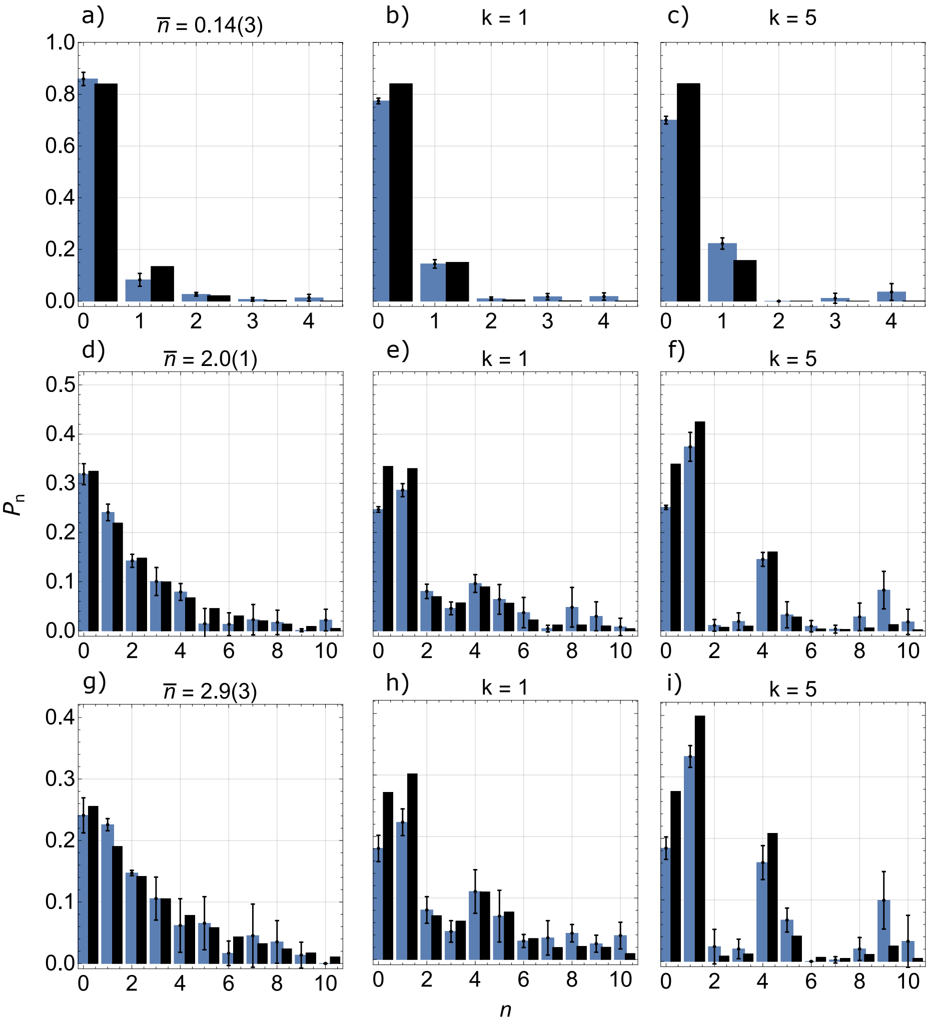

Figure 6.3: Measurement of the repeated phonon absorption for different input thermal energies for $gt = \pi$. States with increasing energy form a more pronounced non-classical modulations, where the solutions corresponding to higher multiples of $gt = l\pi$ become evident. The errors correspond to a single standard deviation resulting from statistical evaluation of five independent measurements. Theoretical simulation including the simulation of the effect of projection noise is depicted by black bars.

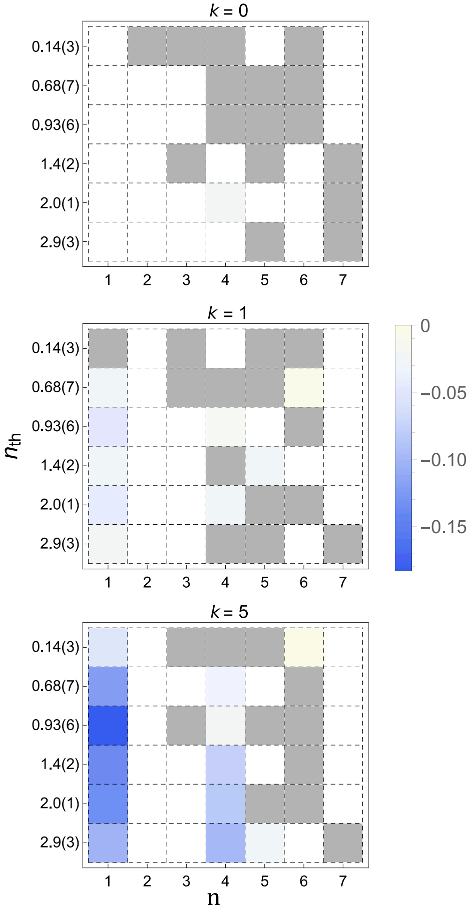

Figure 6.4: Matrices of estimated Klyshko non-classicality criteria. The vertical axis denotes the initial thermal energies of states $\overline{n}_{th}$. The horizontal variable n has a meaning of the Klyshko criteria order. From left to right, the plots show the results for initial thermal states ($k = 0$), distributions undergoing a subtraction of single phonon ($k = 1$), and finally the accumulation of five subtraction processes ($k = 5$). The grey squares show results, where small negative value was evaluated, which did not exceed the interval of a single standard deviation. For all the employed initial thermal states, except for the one with lowest energy, we observe the effect of non-classicality growth as a function o k.

7. Conclusions

The presented work provides a complex set of experimental measurements which focuses on generation and characterization of quantum states implemented on motional degree of freedom of the trapped ion system. We employed the broadly used method of phonon addition and subtraction at 1^{st} motional sidebands [17], and we extended it's application to create complex statistical mixtures. We have used the criteria of non-classicality and genuine quantum non-Gaussianity to characterize the quantum states and analyzed their robustness to the addition of thermal energy. We have further proved that initial thermal energy can be beneficial for the observable non-classical features, which is in contrast with conventional intuition on conditions for sources of nonclassicality to be well isolated from the surrounding environment.

We have focused on generation of high number states and we probed their properties while undergoing the controllable thermalization. We have applied the specifically developed hierarchy of quantum non-Gaussianity criteria [2, 4], which provides a tool to qualitatively express the amount of non-classical features which are being present in the phonon population distribution. We measured and evaluated the depth of the quantum non-Gaussian features, which characterizes the minimal amount of thermal energy added to the system to destroy the observability of quantum state's non-Gaussianity. We additionally performed the controllable experimental heating of ion to precisely calibrate this effect on mechanical system. For the most robust state $|1\rangle$, we have measured the limiting energy preserving the non-Gaussian properties as $\overline{n} = 0.31$, while for increasing energy of measured number states, this gradually drops down to the energy of 0.02 phonons measured for number state $|10\rangle$.

The second experiment extends the method of motional engineering to application of repetitive anti Jaynes-Cummings interactions. We have implemented the scheme, which was theoretically proposed already in 1995 by Blatt et. al. [34] and within the best of our knowledge, it was not experimentally verified up to date. We have shown that the repetitive application of fixed length pulse on the blue axial sideband leads to the dynamical accumulation of motional population into a particular number state, which can be controllably tuned by varying the length gt of the employed interaction pulse. Crucially, this generation method manages to overcome the fundamental requirement of majority of other protocols for preparation of Fock states, which is the minimization of the initial state entropy.

In the last presented experiment we demonstrated the accumulation of non-classicality by addressing the red motional sideband. The point of the demonstrated physics lies in the possibility to generate a non-classical quantum state even by the absorption of phonon, which is in striking contrast to photon annihilation process in photonic quantum systems. We have proved that the presence of non-classical and quantum non-Gaussian features is directly driven by increasing energy of initial thermal state. For various thermal distributions at input, we estimated the resulting distributions after a single and five repetitive phonon absorptions, and we proved that estimated entanglement potential grows with the initial thermal energy. The estimated hierarchy of Klyshko criteria illustrated increase of non-classicality with thermal energy and number of iterations, and also shows the convergence of the distribution towards the number states $|1\rangle$ and $|4\rangle$, which corresponds to a theoretical prediction calculated for many phonon absorptions.

8. Shrnutí v českém jazyce

Předkládaná práce prezentuje sadu provedených experimentálních měření, která se zaměřují na generaci a charakterizaci mechanických kvantových stavů atomu v Paulově pasti. Byly provedeny experimentální postupy využívající přidání a odečet fononu na prvním pohybovém sidebandu. S využitím této metody se podařilo vytvořit komplexní směsi pohybových stavů, které byly následně charakterizovány pomocí metod měření neklasičnosti a kvantové ne-Gaussovosti. Pomocí těchto metod byla také měřena robustnost vytvořených stavů vůči šumu a zvyšujícímu se množství termální energie. Také bylo dokázáno, že tato energie je v určitých případech zdrojem samotné neklasičnosti, tedy že výsledné množství neklasických vlastností se s energií může zvyšovat.

První z prezentovaných experimentů demonstruje tvorbu Fockových stavů pohybu s vysokou energií a měření jejich robustnosti vůči šumu pomocí hierarchie kritérií kvantové negaussovosti. Druhý experiment využívá metodu opakované anti-Jaynes-Cummings interakce na prvním modrém axiálním sidebandu k vytvoření neklasických stavů z počátečního termálního stavu s vysokou energií. Třetí a poslední prezentovaný experiment demonstruje podobný efekt dosažený pomocí inverzní Jaynes-Cummings operace na prvním červeném axiálním sidebandu, kde výsledná neklasičnost je generována pomocí absorpce fononu.

References

1 R. J. Glauber:
'Coherent and incoherent states of the radiation field',
Physical Review **131**, 2766 (1963).

2 R. Filip and L. Mišta Jr:
'Detecting quantum states with a positive wigner function beyond mixtures of gaussian states',
Physical review letters **106**, 200401 (2011).

3 I. Straka, L. Lachman, J. Hloušek, M. Miková, M. Mičuda, M. Ježek and R. Filip:
'Quantum non-gaussian multiphoton light',
npj Quantum Information **4**, 1–5 (2018).

4 L. Lachman, I. Straka, J. Hloušek, M. Ježek and R. Filip:
'Faithful hierarchy of genuine n-photon quantum non-gaussian light',
Physical review letters **123**, 043601 (2019).

5 F. Wolf, C. Shi, J. C. Heip, M. Gessner, L. Pezzè, A. Smerzi, M. Schulte, K. Hammerer and P. O. Schmidt:
'Motional fock states for quantum-enhanced amplitude and phase measurements with trapped ions',
Nat. Commun. **10**, 1–8 (2019).

6 K. C. McCormick, J. Keller, S. C. Burd, D. J. Wineland, A. C. Wilson and D. Leibfried:
'Quantum-enhanced sensing of a single-ion mechanical oscillator',
Nature **572**, 86–90 (2019).

7 M. Gessner, A. Smerzi and L. Pezzè:
'Metrological nonlinear squeezing parameter',
Phys. Rev. Lett. **122**, 090503 (2019).

8 C. Flühmann, T. L. Nguyen, M. Marinelli, V. Negnevitsky, K. Mehta and J. P. Home:
'Encoding a qubit in a trapped-ion mechanical oscillator',
Nature **566**, 513 (2019).

9 M. H. Michael, M. Silveri, R. Brierley, V. V. Albert, J. Salmilehto, L. Jiang and S. M. Girvin:
'New class of quantum error-correcting codes for a bosonic mode',
Physical Review X **6**, 031006 (2016).

10 L. Hu, Y. Ma, W. Cai, X. Mu, Y. Xu, W. Wang, Y. Wu, H. Wang, Y. Song, C.-L. Zou et al.:
'Quantum error correction and universal gate set operation on a binomial bosonic logical qubit',
Nature Physics **15**, 503–508 (2019).

11 P. Campagne-Ibarcq, A. Eickbusch, S. Touzard, E. Zalys-Geller, N. E. Frattini, V. V. Sivak, P. Reinhold, S. Puri, S. Shankar, R. J. Schoelkopf et al.:
'Quantum error correction of a qubit encoded in grid states of an oscillator',
Nature **584**, 368–372 (2020).

12 A. GHOSH, W. NIEDENZU, V. MUKHERJEE and G. KURIZKI:
'Thermodynamic principles and implementations of quantum machines',
Thermodynamics in the Quantum Regime: Fundamental Aspects and New Directions, edited by F. Binder, LA Correa, C. Gogolin, J. Anders, and G. Adesso (Springer International Publishing, Cham, 2018) pp, 37–66 (2018).

13 G. MASLENNIKOV, S. DING, R. HABLÜTZEL, J. GAN, A. ROULET, S. NIMMRICHTER, J. DAI, V. SCARANI and D. MATSUKEVICH:
'Quantum absorption refrigerator with trapped ions',
Nature communications **10**, 1–8 (2019).

14 M.-L. CAI, Z.-D. LIU, W.-D. ZHAO, Y.-K. WU, Q.-X. MEI, Y. JIANG, L. HE, X. ZHANG, Z.-C. ZHOU and L.-M. DUAN:
'Observation of a quantum phase transition in the quantum rabi model with a single trapped ion',
Nature communications **12**, 1–8 (2021).

15 L. PODHORA, T. PHAM, A. LEŠUNDÁK, P. OBŠIL, M. ČÍŽEK, O. ČÍP, P. MAREK, L. SLODIČKA and R. FILIP:
'Unconditional accumulation of nonclassicality in a single-atom mechanical oscillator',
Advanced Quantum Technologies **3**, 2000012 (2020).

16 L. PODHORA, L. LACHMAN, T. PHAM, A. LE ŠUNDÁK, O. ČÍP, L. SLODI ČKA and R. FILIP:
'Quantum non-gaussianity of multiphonon states of a single atom',
Phys. Rev. Lett. **129**, 013602 (2022).

17 D. LEIBFRIED, R. BLATT, C. MONROE and D. WINELAND:
'Quantum dynamics of single trapped ions',
Reviews of Modern Physics **75**, 281 (2003).

18 C. BLOCKLEY, D. WALLS and H. RISKEN:
'Quantum collapses and revivals in a quantized trap',
EPL (Europhysics Letters) **17**, 509 (1992).

19 C. ROOS:
'Controlling the quantum state of trapped ions',
PhD thesis (2000).

20 R. BONIFACIO, S. OLIVARES, P. TOMBESI and D. VITALI:
'Model-independent approach to nondissipative decoherence',
Physical Review A **61**, 053802 (2000).

22 L. DAVIDOVICH:
'Sub-poissonian processes in quantum optics',
Reviews of Modern Physics **68**, 127 (1996).

23 U. CHABAUD, D. MARKHAM and F. GROSSHANS:
'Stellar representation of non-gaussian quantum states',
Physical Review Letters **124**, 063605 (2020).

24 P. OBŠIL:
'Nonclassical and coherent emission from trapped ion crystals',
PhD thesis (2021).

25 A. LEŠUNDÁK:
'Distance measurements with mode-filtered frequency comb and analysis of fluorescence from trapped ion at modulated dark state',
PhD thesis (2019).

26 D. LEIBFRIED, D. MEEKHOF, B. KING, C. MONROE, W. M. ITANO and D. J. WINELAND:
'Experimental determination of the motional quantum state of a trapped atom',
Phys. Rev. Lett. **77**, 4281 (1996).

27 G. Araneda:
'Experiments with single photons emitted by single atoms',
PhD thesis (2019).

28 J. Eschner, G. Morigi, F. Schmidt-Kaler and R. Blatt:
'Laser cooling of trapped ions',
JOSA B **20**, 1003–1015 (2003).

29 G. Morigi, J. Eschner and C. H. Keitel:
'Ground state laser cooling using electromagnetically induced transparency',
Physical review letters **85**, 4458 (2000).

30 F. Diedrich, J. Bergquist, W. M. Itano and D. Wineland:
'Laser cooling to the zero-point energy of motion',
Physical review letters **62**, 403 (1989).

31 B. Srivathsan, M. Fischer, L. Alber, M. Weber, M. Sondermann and G. Leuchs:
'Measuring the temperature and heating rate of a single ion by imaging',
New Journal of Physics **21**, 113014 (2019).

32 G. Cerchiari, G. Araneda, L. Podhora, L. Slodička, Y. Colombe and R. Blatt:
'Measuring ion oscillations at the quantum level with fluorescence light',
Physical Review Letters **127**, 063603 (2021).

33 D. Klyshko:
'Observable signs of nonclassical light',
Physics Letters A **213**, 7–15 (1996).

34 R. Blatt, J. Cirac and P. Zoller:
'Trapping states of motion with cold ions',
Physical Review A **52**, 518 (1995).